Research Square

Preprints are preliminary reports that have not undergone peer review.
They should not be considered conclusive, used to inform clinical practice,
or referenced by the media as validated information.

Plasmodium falciparum derived small extracellular vesicles from infected erythrocytes show distinct RNA and protein cargo signatures with potential as malaria biomarkers

Muna Abubaker
University of Salford
Berna Sayan
University of Salford
Toby Aarons
University of Salford
Niroshini Nirmalan
University of Salford
Arijit Mukhopadhyay
a.mukhopadhyay@salford.ac.uk
University of Salford

Research Article

Keywords: Plasmodium falciparum, Malaria, Small extracellular vesicles, Infected erythrocytes, Ribosomal RNA, Parasite-derived proteins, Biomarkers

Posted Date: November 23rd, 2026

DOI: https://doi.org/10.21203/rs.3.rs-11731263/v1

License: This work is licensed under a Creative Commons Attribution 4.0 International License.
Read Full License

Additional Declarations: No competing interests reported.

Plasmodium falciparum derived small extracellular vesicles from infected erythrocytes show distinct RNA and protein cargo signatures with potential as malaria biomarkers

Muna Abubaker[1], Berna S. Sayan[1], Toby Aarons[1], Niroshini Nirmalan[1]*, Arijit Mukhopadhyay[1]*

1, Translational Medicine Laboratory, Faculty of Health, Community and Life Sciences, University of Salford, United Kingdom

*** - Corresponding Authors**

Prof Arijit Mukhopadhyay: Faculty of Health Community and Life Sciences, University of Salford, Room 322 Peel Building, The Crescent, M5 4WT, United Kingdom. E-mail: a.mukhopadhyay@salford.ac.uk; ORCID: https://orcid.org/0000-0002-1089-7179

(all communications should be with Prof Mukhopadhyay)

Prof Niroshini Nirmalan: Faculty of Science Engineering and Environment, University of Salford, Peel Building, The Crescent, M5 4WT, United Kingdom. E-mail: N.J.Nirmalan@salford.ac.uk; ORCID: https://orcid.org/0000-0001-9000-298X

Abstract

Background: Small extracellular vesicles (sEVs) are increasingly recognised as mediators of host-pathogen communication and potential malaria biomarkers. However, changes in their abundance and molecular composition throughout the *Plasmodium falciparum* intraerythrocytic developmental cycle remain poorly understood. This study investigated developmental-stage-associated changes in sEV abundance, membrane phenotype and molecular cargo.

Methods: Small EVs were isolated from synchronised *P. falciparum*-infected red blood cells (iRBCs) at the ring, trophozoite and schizont stages and uninfected red blood cells (uRBCs) using differential centrifugation and size-exclusion chromatography. Vesicles were characterised by nanoparticle tracking analysis (NTA), transmission electron microscopy and fluorescence NTA. Protein content was assessed by BCA assay and western blotting, while parasite-specific 18S and 28S ribosomal RNAs (rRNAs) were quantified by RT-qPCR.

Results: NTA revealed increased particle abundance in iRBC-derived preparations, from approximately 2.4×10^{10} particles in uRBC controls to 8×10^{10} in ring- and trophozoite-derived preparations, reaching 1.2×10^{11} at the schizont stage. In schizont-stage cultures, particle abundance increased 3.5-fold as parasitaemia increased from 1 to 4%. Most particles (70-88%) were ≤200 nm. Total protein concentration was highest in schizont-derived preparations (approximately 4.0 µg/µL; $P < 0.0001$). Fluorescence NTA revealed higher CMO-positive proportions in iRBC-derived preparations (30-40%) than in uRBC controls (10%). Within CMO-positive populations, CD63-positive vesicles decreased from approximately 65% at the ring and trophozoite stages to 18% at the schizont stage, whereas CD9-positive vesicles increased to approximately 60%. *Plasmodium* aldolase and histidine-rich protein 2 (HRP2) were detected exclusively in iRBC-derived sEVs, with strongest signals at the schizont and ring stages, respectively. Parasite-specific 18S and 28S rRNAs remained detectable following Proteinase K and RNase A treatment, with highest relative abundance in schizont-derived preparations.

Conclusions: *P. falciparum* infection is associated with developmental-stage-dependent changes in sEV abundance, membrane phenotype and molecular cargo. Distinct parasite-derived protein and tetraspanin profiles, together with protected parasite-specific rRNAs, support further investigation of sEV-associated molecular signatures as potential biomarkers of malaria infection and parasite developmental stage.

Keywords: *Plasmodium falciparum*; Malaria; Small extracellular vesicles; Infected erythrocytes; Ribosomal RNA; Parasite-derived proteins; Biomarkers.

Introduction

Malaria remains one of the world's most important infectious diseases and continues to impose a substantial burden of morbidity and mortality, particularly in low- and middle-income countries. Rapid and accurate diagnosis is essential for effective case management, surveillance and disease control. Despite considerable progress in malaria control programmes, *Plasmodium falciparum* continues to account for the majority of malaria-associated deaths worldwide, with young children and pregnant women being disproportionately affected [1]. Microscopy, rapid diagnostic tests (RDTs) and nucleic acid-based assays have substantially improved malaria diagnosis. However, each approach has important limitations. Microscopy is labour-intensive and highly dependent on operator expertise, HRP2-based RDTs may yield false-positive or false-negative results because of persistent circulating antigen or *pfhrp2/pfhrp3* gene deletions, and molecular assays generally require specialised laboratory infrastructure that is often unavailable in resource-limited settings [2,3]. Consequently, there remains a need to identify novel biomarkers that are sensitive, specific, minimally invasive and applicable across diverse clinical and field settings.

Beyond improving diagnosis, a major challenge in malaria research is to better understand the molecular mechanisms governing host–parasite interactions throughout infection. *Plasmodium falciparum*, the most virulent human malaria parasite, causes severe complications, including cerebral malaria, which remains a major cause of malaria-associated mortality [4,5]. Cerebral malaria is characterised by the sequestration of infected erythrocytes within the cerebral microvasculature through cytoadherence. This process is mediated by parasite-induced remodelling of the erythrocyte membrane and adhesion to endothelial receptors, including intercellular adhesion molecule-1 (ICAM-1), CD36 and endothelial protein C receptor (EPCR) [4-7]. Although the parasite ligands and host receptors involved in cytoadherence have been extensively characterised, the signalling mechanisms that coordinate communication between infected erythrocytes, neighbouring host cells and the vascular endothelium remain incompletely understood [4-7]. A better understanding of these mechanisms could provide important insights into malaria pathogenesis while identifying molecular signatures associated with parasite biology, disease progression and clinical outcome.

Extracellular vesicles (EVs) have emerged as important mediators of intercellular communication and promising sources of disease-associated biomarkers. EVs are lipid bilayer-

enclosed particles released by virtually all cell types into biological fluids. They transport proteins, lipids, metabolites and nucleic acids that reflect the physiological or pathological state of their cell of origin [8-10]. Their stability in biological fluids and ability to protect biomolecules from enzymatic degradation have generated considerable interest in their use as minimally invasive biomarkers for cancer, cardiovascular disease, inflammatory disorders and infectious diseases [11,12]. Beyond their diagnostic potential, EVs facilitate cell-to-cell communication through the transfer of biologically active molecules capable of altering the phenotype and function of recipient cells, making them attractive candidates for investigating host–pathogen interactions [8-12].

Interest in the role of extracellular vesicles during malaria infection has increased substantially over the past decade. During *P. falciparum* infection, EVs are released by both host cells and infected erythrocytes and are increasingly recognised as important mediators of parasite–parasite and parasite–host communication [13-16]. Vesicles released from infected erythrocytes contain parasite-derived proteins, lipids and nucleic acids that can be transferred to neighbouring infected erythrocytes, endothelial cells and immune cells, influencing parasite development, immune activation and vascular function [14-17]. EV-mediated communication has also been implicated in parasite population synchronisation, gametocyte commitment and modulation of host inflammatory responses, highlighting its potential contribution to malaria pathogenesis [14-18]. Furthermore, parasite-derived EVs can activate endothelial and innate immune cells, raising the possibility that EV-mediated signalling contributes to the vascular dysfunction associated with severe malaria, although the underlying mechanisms remain to be fully elucidated [15-19].

Among the heterogeneous populations of extracellular vesicles, small extracellular vesicles (sEVs) have attracted particular interest because of their nanoscale size, stability and rich molecular composition. Their protein and nucleic acid content reflects both the cellular origin and physiological state of the releasing cell, making them attractive candidates for minimally invasive biomarker discovery [9-12]. Proteomic analyses of malaria-derived sEVs have identified both host- and parasite-derived proteins, including membrane-remodelling proteins, invasion-associated proteins, metabolic enzymes and other virulence-associated factors [20,21]. Likewise, parasite-derived nucleic acids associated with sEVs have emerged as promising diagnostic targets because vesicle encapsulation may protect them from degradation while preserving molecular information related to parasite development and infection status

[17,19]. Together, these findings suggest that sEVs provide a stable and biologically informative source of molecular signatures for both malaria diagnosis and the study of parasite biology.

Despite these advances, several important questions remain unresolved. First, because extracellular vesicles released during malaria infection originate from multiple cellular sources, defining the cellular origin and biological significance of their molecular content remains challenging, particularly in clinical samples containing vesicles derived from leukocytes, platelets and endothelial cells alongside those released from infected erythrocytes. This complexity complicates the identification of parasite-specific molecular signatures and may obscure biologically relevant signals. Second, although sEV release from *P. falciparum*-infected erythrocytes has been demonstrated, relatively little is known about how vesicle abundance, membrane composition and molecular content change throughout the intraerythrocytic developmental cycle. Finally, although parasite-derived nucleic acids associated with sEVs have attracted increasing interest, few studies have systematically investigated whether specific vesicle-associated RNAs exhibit stage-dependent abundance patterns that could serve as biomarkers or provide insight into host–parasite communication during infection.

These questions are particularly important because erythrocyte-derived sEVs occupy a unique biological context. Mature erythrocytes are enucleated and lack ribosomes, endosomes and conventional secretory machinery. Consequently, vesicles released from infected erythrocytes raise an important biological question: do they simply represent by-products of membrane damage and cellular stress, or do they reflect a regulated, parasite-associated process linked to parasite development and host-cell remodelling? Understanding these processes is important not only for investigating the biology of *P. falciparum* infection but also for determining whether sEV-associated molecular signatures could provide biologically meaningful indicators of parasite activity.

Of particular interest are parasite-derived ribosomal RNAs (rRNAs), which may represent potential molecular biomarkers of *P. falciparum* infection. Unlike many eukaryotes, *P. falciparum* lacks the canonical RNA interference machinery required for endogenous microRNA biogenesis [22,23]. In contrast, parasite-specific rRNAs are abundant and may provide useful indicators of parasite presence and developmental stage. Their association with sEVs may also offer protection against extracellular degradation, potentially enhancing their

suitability as stable molecular biomarkers. Understanding whether parasite-specific rRNAs are associated with sEVs throughout the intraerythrocytic developmental cycle may therefore contribute to the identification of stage-associated molecular signatures.

In this study, we investigated whether sEVs released from *P. falciparum*-infected erythrocytes exhibit developmental-stage-associated changes in vesicle abundance, membrane phenotype and molecular cargo, with particular emphasis on parasite-derived proteins and 18S and 28S rRNAs. We hypothesised that these characteristics vary during parasite maturation and may provide molecular signatures associated with parasite development. By addressing these knowledge gaps, this study aims to improve our understanding of malaria-derived sEVs and provide a foundation for further investigation of their potential as biomarkers of *P. falciparum* infection and their involvement in host–parasite communication.

Materials and Methods

Plasmodium falciparum culture and synchronisation

Plasmodium falciparum K1 strain parasites were maintained *in vitro* under sterile conditions in an ESCO Class II biological safety cabinet using standard aseptic techniques. Parasites were cultured in human red blood cells (RBCs) at 5% haematocrit in complete RPMI 1640 medium containing 25 mM HEPES and L-glutamine, supplemented with 2.5 g bovine serum albumin, 2.5 mL hypoxanthine (1 mg/mL in phosphate-buffered saline [PBS]), 0.5 mL gentamicin (50 mg/mL in PBS), and 2.5 mL of 40% glucose per 500 mL medium. Cultures were incubated at 37°C under a gas mixture of 5% CO2, 5% O2 and 90% N2.

Whole blood (Type O+, obtained from NHS Blood bank) was washed before use to remove plasma, preservatives and leukocytes. Blood was centrifuged at 1200 × *g* for 5 min, and the plasma and buffy coat were removed. The washing step was repeated at least three times using

RPMI 1640 without supplements. Washed RBCs were then resuspended in complete medium to 50% haematocrit and stored at 2-8°C until use.

Parasitaemia was monitored by Giemsa-stained thin blood smears. Thin films were fixed in 100% methanol, stained with 10% Giemsa for 20 min, and examined under oil immersion using a Leica DM500 microscope. Parasitaemia was calculated as the percentage of infected RBCs among total RBCs counted, with at least three fields analysed per slide.

Parasite cultures were synchronised using 5% D-sorbitol. Cultures with parasitaemia > 2% and predominantly ring-stage parasites were centrifuged at 1200 × *g* for 5 min, resuspended in 5% sorbitol, and incubated at room temperature for 5 min. After centrifugation, pellets were washed three times in complete medium and resuspended at 50% haematocrit. For extracellular vesicle experiments, parasites were double-synchronised by repeating sorbitol treatment after 6 h to obtain tightly synchronised ring-stage cultures. Ring-stage cultures were then incubated for 24-30 h or 36-42 h to generate trophozoite and schizont-stage cultures, respectively.

Isolation and purification of small extracellular vesicles

Small extracellular vesicles (sEVs) were isolated from conditioned culture medium (CCM) of double-synchronised infected RBC (iRBC) cultures and uninfected RBC (uRBC) controls using differential centrifugation, precipitation and size-exclusion chromatography (SEC).

Ring, trophozoite and schizont-stage cultures were established at an initial parasitaemia of 4%, and CCM was collected after 48 h. To assess the effect of parasite density on vesicle production, schizont-stage cultures were also set up at parasitaemia levels ranging from 1% to 4%, and CCM was collected after 48 h. Control CCM was collected from uRBC cultures maintained under the same conditions.

Conditioned medium was first centrifuged at 1000 × *g* for 10 min to remove intact cells and large debris, followed by centrifugation at 2000 × *g* for 10 min. The supernatant was then filtered through a 0.22 μm filter and centrifuged at 10,600 × *g* for 48 min. Cell Exo-spin buffer (Cell Guidance Systems, Cambridge, UK) was added to the supernatant at a 2:1 sample-to-buffer ratio, mixed by inversion, and incubated overnight at 4°C. Samples were then centrifuged at 10,600 × *g* for 96 min. After careful removal of the supernatant, the pellet was

resuspended in PBS, transferred to a microcentrifuge tube, centrifuged again at 10,600 × *g* for 10 min, and finally resuspended in 100 µL PBS.

For further purification, precipitated vesicles were subjected to SEC using the Exo-spin sEV isolation and purification kit (Cell Guidance Systems, UK). Columns were equilibrated to room temperature, washed twice with 250 µL PBS, and loaded with 100 µL of resuspended vesicle sample. After entry of the sample into the column matrix, the flow-through was discarded. Vesicles were then eluted with 200 µL PBS by centrifugation at 50 × *g* for 60 s. Protease inhibitor was added at 1 µL per 100 µL sample, and purified sEVs were stored at -80°C until analysis.

Nanoparticle tracking analysis

Particle size distribution and concentration were determined using a ZetaView nanoparticle tracking analyser (Particle Metrix, Germany) according to the manufacturer's instructions. The instrument was calibrated with 100 nm polystyrene beads diluted 1:10,000 in distilled water. Before each run, the system was flushed with sterile PBS.

Samples were diluted in PBS, typically starting at 1:1000, and analysed in scatter mode at 520 nm. Measurements were recorded at 25°C across 11 camera positions. Instrument settings were as follows: sensitivity 80 and shutter speed 200. Video data were analysed using ZetaView software to determine particle size distribution, particle concentration and total particle counts based on Brownian motion. After analysis, the instrument was flushed thoroughly with deionised water.

Fluorescent nanoparticle tracking analysis

Fluorescent nanoparticle tracking analysis (fNTA) was performed using the ZetaView single-laser system (Particle Metrix, Germany) to assess membrane-bound vesicles and vesicle subpopulations positive for CD9, CD63 and CD81. The instrument was calibrated using 100 nm fluorescent polystyrene beads diluted 1:500,000 in distilled water.

Following conventional NTA, samples were diluted in PBS to achieve approximately 150-200 particles per frame. Vesicles were labelled with PE/Dazzle anti-human CD9, CD63 and CD81 antibodies (BioLegend, UK, 10626D, 10628D and 10630D), and with CellMask Orange (CMO; Invitrogen, UK) according to the manufacturers' instructions. For CMO staining, dye was serially diluted to 1:10,000,000 in PBS and added to samples at a 9:1 ratio (9 µL sample:1 µL diluted dye). For antibody staining, CD markers were diluted 1:100,000 in PBS, and 1 µL diluted antibody was added to 9 µL sample. Samples were incubated in the dark for 1 h at room temperature.

After incubation, labelled samples were diluted 1:1000 in PBS and analysed with the 550 nm fluorescence filter. The concentration of fluorescent particles was determined, and the percentage of tetraspanin-positive vesicles was calculated relative to the CMO-positive membrane-bound vesicle population.

Transmission electron microscopy

To assess vesicle morphology, 10 µL aliquots of purified sEVs from infected and uninfected RBC cultures were prepared for transmission electron microscopy (TEM). Samples were adsorbed onto carbon-coated grids, washed with PBS, and fixed with 1% glutaraldehyde. Grids were washed with deionised water and stained with 1% uranyl acetate, followed by a second staining step in a 1:9 mixture of 4% uranyl acetate and 2% methyl cellulose at 4°C for 10 min. Samples were then dehydrated through a graded alcohol series and imaged using a FEI Tecnai G2 Spirit BioTwin transmission electron microscope operated at 120 kV.

Total protein quantification

Total protein concentration in purified sEV samples was determined using the bicinchoninic acid (BCA) assay (Thermo Scientific, UK) according to the manufacturer's instructions. Working reagent was prepared fresh by mixing reagents A and B at a 50:1 ratio. Bovine serum albumin (BSA) standards ranging from 0 to 2000 µg/mL were prepared in PBS. sEV samples were diluted 1:10 in PBS.

A volume of 25 µL of each standard or sample was added in triplicate to a 96-well plate, followed by 175 µL working reagent. Plates were incubated at 37°C for 30 min with shaking,

and absorbance was measured at 562 nm using a microplate reader. Protein concentrations were calculated from the BSA standard curve.

Western blotting

For immunoblot analysis, 20 µg of total vesicle protein was mixed with loading buffer containing dithiothreitol (DTT), heated at 95°C for 5 min, and loaded onto precast polyacrylamide gels (Bio-Rad). Following electrophoresis, proteins were transferred to nitrocellulose membranes overnight at 20V at 4°C. Membranes were then blocked for 1 h at room temperature in PBS containing 0.1% Tween and 5% skimmed milk.

Primary antibodies were prepared in blocking buffer at the following dilutions: anti-P. falciparum HRP2 (Abcam, ab38905), 1:1000; anti-Plasmodium aldolase (Abcam, ab207494), 1:1000; anti-flotillin-1 (Proteintech, 67968-1-Ig), 1:2000; and anti-GM130 (Proteintech, 66662-1-Ig), 1:10,000. Membranes were incubated with the respective primary antibodies for 1 h at room temperature, followed by three washes of 10 min each with washing buffer. Membranes were then incubated for 1 h at room temperature with HRP-conjugated polyclonal goat anti-rabbit (Dako, P0448) or goat anti-mouse (Dako, P0447) secondary antibodies, as appropriate. As the *Plasmodium* aldolase primary antibody was directly conjugated to HRP, no secondary antibody was required for its detection.

Chemiluminescent detection was performed using SuperSignal™ West Atto Ultimate Sensitivity Substrate (Thermo Fisher Scientific) for flotillin-1 and SuperSignal™ West Femto Maximum Sensitivity Substrate (Thermo Fisher Scientific) for GM130, HRP2 and *Plasmodium* aldolase. Membranes were imaged using the Odyssey XF Imaging System (LI-COR Biosciences).

Total RNA extraction from small extracellular vesicles

Total RNA was extracted from ring-, trophozoite- and schizont-derived sEVs using the miRNeasy Micro Kit (Qiagen, Germany) according to the manufacturer's instructions, with minor modifications. To assess whether the detected RNA was protected within the sEVs, samples were analysed under treated and untreated conditions, using 50 µL of sEV suspension for each condition. Proteinase K + RNase A (1 µL) was added to treated samples to remove external proteins and RNA not protected within the vesicles, while an equivalent volume of

PBS was added to untreated controls. Samples were incubated at 37 °C for 30 min. Subsequently, 0.5 µL of 100× Halt™ and PhosSTOP™ inhibitor solution was added to treated samples, while an equivalent volume of PBS was added to untreated controls. Samples were then incubated on ice for 10 min.

RNA extraction was initiated by adding 700 µL QIAzol Lysis Reagent to each sample, followed by incubation at room temperature for 20 min. Chloroform (90 µL) was then added, and samples were vigorously mixed for 15 s, incubated at room temperature for 2 min, and centrifuged at 12,000 × g for 15 min at 4 °C. The aqueous phase was transferred to a fresh RNase-free tube and mixed with two volumes of 100% ethanol. The mixture was applied to an RNeasy MinElute spin column and washed sequentially with RWT buffer, RPE buffer and 80% ethanol according to the manufacturer's instructions. RNA was eluted in 14 µL RNase-free water and stored at -80 °C until further analysis. RNA extracted from Proteinase K + RNase A-treated sEV samples was used for subsequent cDNA synthesis and RT-qPCR analysis of parasite-specific 18S and 28S rRNAs.

RNA quantification

Total RNA concentration was determined using a NanoDrop spectrophotometer. Small RNA concentration was measured using the Qubit 3.0 Fluorometer (Thermo Fisher Scientific, UK) with the Qubit miRNA Assay Kit according to the manufacturer's instructions. For the Qubit assay, working solution was prepared by diluting the reagent 1:200 in assay buffer. Standards were prepared using 10 µL standard and 190 µL working solution. Samples were prepared by mixing 2 µL RNA with 198 µL working solution, followed by incubation at room temperature for 2 min before measurement.

cDNA synthesis

cDNA synthesis was performed using RNA extracted from Proteinase K + RNase A-treated sEV samples using the QuantiMir™ RT Kit (System Biosciences). The kit uses polyadenylation and anchor oligo(dT) adaptor priming for reverse transcription. First, 5 µL RNA was polyadenylated in a 10 µL reaction containing 5× PolyA buffer, $MnCl_2$, ATP and poly(A) polymerase, followed by incubation at 37 °C for 30 min. Next, 5 µL anchor oligo(dT) adaptor was added, and samples were heated at 60 °C for 5 min and cooled at room temperature for 2 min. Reverse transcription was then carried out by adding RT buffer, dNTP mix, DTT, RNase-free water and reverse transcriptase to a final volume of 20.5 µL. Reactions were

incubated at 42 °C for 60 min, followed by enzyme inactivation at 95 °C for 10 min. Synthesised cDNA was stored at -20 °C.

RT-qPCR detection of P. falciparum 18S and 28S rRNA

RT-qPCR was performed using a Rotor-Gene Q instrument (Qiagen) to detect P. falciparum-specific 18S and 28S rRNAs in cDNA generated from Proteinase K + RNase A-treated sEV samples. The following primers were used:

Pf_18S rRNA
Forward: 5′-GCTCTTTCTTGATTTCTTGGATG-3′
Reverse: 5′-AGCAGGTTAAGATCTCGTTCG-3′

Pf_28S rRNA
Forward: 5′-ACTGAAACGGACAAGGGGAAT-3′
Reverse: 5′-GCAGAAATCACATTGTGTTAATACCA-3′

PCR reactions contained 15 µL 2× SYBR Green Mastermix (Bio-Rad), 1 µL forward primer, 0.5 µL reverse primer, 12.5 µL RNase-free water and 1 µL cDNA template. No-template controls contained RNase-free water instead of cDNA. Thermal cycling conditions were 50 °C for 2 min and 95 °C for 10 min, followed by 40 cycles of 95 °C for 15 s and 60 °C for 1 min. Melt curve analysis was performed from 50 °C to 95 °C.

All reactions were performed in technical triplicate. Relative abundance of P. falciparum-specific 18S and 28S rRNAs was calculated using the 2^−Ct method. Values were scaled by factors of 10^{10} for 18S rRNA and 10^{8} for 28S rRNA and expressed as arbitrary units (AU). Data were obtained from three independent biological replicates (n = 3).

Statistical analysis

All statistical analyses were performed using GraphPad Prism software. Data are presented as mean ± standard deviation (SD) from three independent biological replicates (n = 3). Differences among groups were assessed using ordinary one-way analysis of variance (ANOVA), followed by Tukey's multiple comparisons post hoc test. Statistical significance was defined as $P < 0.05$.

Results

Small EV abundance and protein content increase with *P. falciparum* development and parasitaemia

Nanoparticle tracking analysis (NTA) revealed differences in particle abundance across the *P. falciparum* intraerythrocytic developmental cycle (Fig. 1A). Particle numbers were lowest in uninfected red blood cell (uRBC) preparations (approximately 2.4×10^{10} particles) and increased to approximately 8×10^{10} particles in both ring- and trophozoite-stage infected red blood cell (iRBC) preparations. The highest particle number was observed in schizont-derived preparations (approximately 1.2×10^{11} particles), representing a fivefold increase compared with uRBC controls.

To investigate the association between particle abundance and parasite density, particle numbers were assessed in schizont-stage cultures at parasitaemia levels ranging from 1% to 4% (Fig. 1B). Particle numbers increased progressively with increasing parasitaemia, from approximately 8×10^{10} particles at 1% to 1.3×10^{11}, 1.7×10^{11} and 2.8×10^{11} particles at 2%, 3% and 4% parasitaemia, respectively. This represents an approximately 3.5-fold increase between 1% and 4% parasitaemia.

Analysis of particle size distribution showed that the majority of particles were ≤200 nm, accounting for approximately 70–88% of detected particles across the preparations (Fig. 1C). The highest proportion was observed in schizont-derived preparations (approximately 88%), followed by ring-derived preparations (approximately 85%), while uRBC and trophozoite preparations showed similar proportions (approximately 70–72%). Transmission electron microscopy (TEM) further confirmed the presence of vesicular structures in both uRBC- and iRBC-derived preparations (Fig. 1D).

Total protein concentration also varied across the developmental stages (Fig. 1E). Protein concentration increased from approximately 0.7 µg/µL in uRBC-derived preparations to 2.1 µg/µL and 2.0 µg/µL in ring- and trophozoite-derived preparations, respectively. The highest concentration was observed in schizont-derived preparations (approximately 4.0 µg/µL). Protein concentration was significantly higher in ring-derived preparations than in uRBC

controls ($P < 0.0001$), whereas no significant difference was observed between ring- and trophozoite-derived preparations. Schizont-derived preparations showed significantly higher protein concentrations than uRBC, ring- and trophozoite-derived preparations ($P < 0.0001$).

Together, these findings indicate that *P. falciparum* infection is associated with increased particle abundance and protein content, with the highest levels observed in schizont-derived preparations. Particle abundance also increased with increasing parasitaemia in schizont-stage cultures.

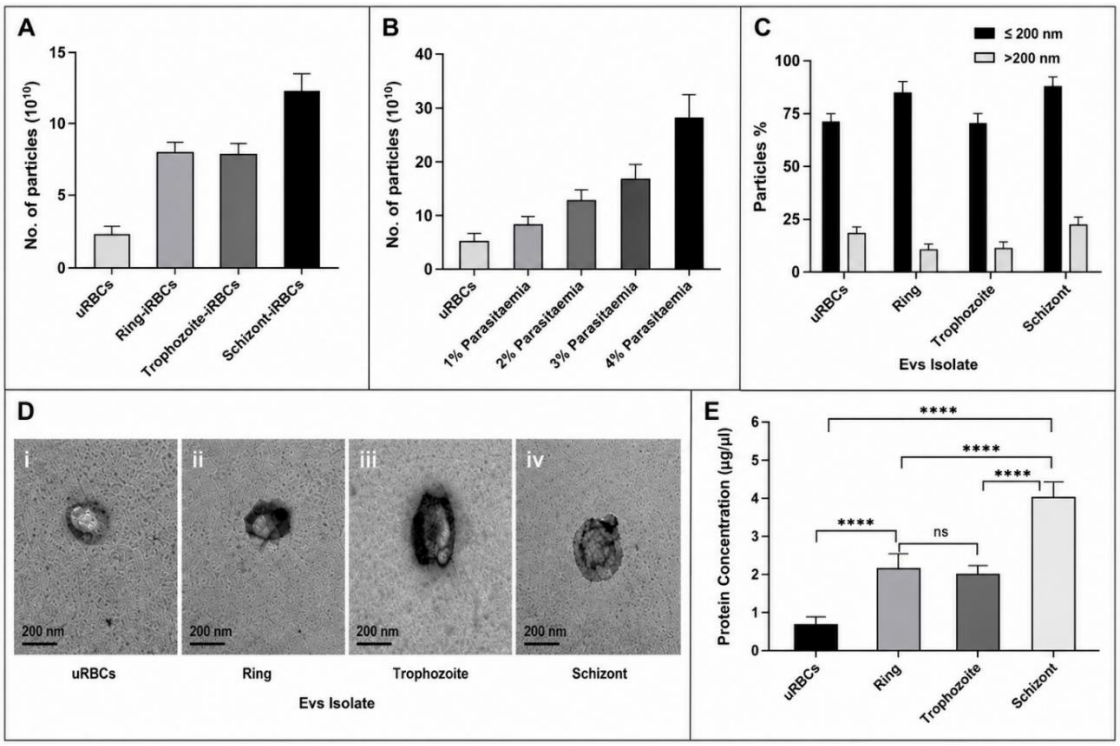

Figure 1. Characterisation of small extracellular vesicles derived from *Plasmodium falciparum*-infected erythrocytes across the intraerythrocytic developmental cycle. (A) Particle numbers in small extracellular vesicle (sEV) preparations derived from uninfected red blood cells (uRBCs) and *P. falciparum*-infected red blood cells (iRBCs) at the ring, trophozoite and schizont stages, determined by nanoparticle tracking analysis (NTA). **(B)** Particle numbers in sEV preparations isolated from schizont-stage cultures at increasing parasitaemia levels (1-4%), with uRBC-derived preparations included as controls. **(C)** Percentage distribution of particles ≤200 nm and >200 nm in sEV preparations from uRBCs and ring-, trophozoite- and schizont-stage iRBC cultures. **(D)** Representative transmission electron microscopy (TEM) images of sEV preparations derived from **(i)** uRBCs and iRBCs at the **(ii)** ring, **(iii)** trophozoite and **(iv)** schizont stages. Scale bars = 200 nm. **(E)** Total protein concentration (µg/µL) measured by BCA assay in sEV preparations derived from uRBCs and ring-, trophozoite- and schizont-stage iRBC cultures, without Proteinase K treatment. Data are presented as mean ± SD from three independent biological replicates (n = 3). Statistical analysis was performed using one-way ANOVA followed by Tukey's multiple comparisons test; ns, not significant; ****P < 0.0001.

Membrane-bound and tetraspanin-positive sEV populations vary across *P. falciparum* developmental stages

Fluorescence nanoparticle tracking analysis (fNTA) was used to characterise membrane-bound particles and tetraspanin-positive sEV populations. CellMask Orange (CMO) labelling revealed a higher proportion of membrane-bound particles in sEV preparations derived from *P. falciparum*-infected red blood cells (iRBCs) compared with uninfected red blood cell (uRBC) controls (Fig. 2A). The proportion of CMO-positive particles varied across parasite developmental stages, accounting for approximately 30-45% of total particles in iRBC-derived preparations compared with approximately 10% in uRBC-derived preparations. These percentages were calculated relative to the total particle concentration measured in scatter mode (520 nm) for each preparation and therefore represent the proportion of membrane-labelled particles rather than their absolute abundance.

Analysis of the tetraspanins CD9, CD63 and CD81 revealed distinct stage-associated patterns (Fig. 2B). CD63-positive vesicles represented approximately 65% of CMO-positive particles at the ring and trophozoite stages but decreased to approximately 18% at the schizont stage. In contrast, the proportion of CD9-positive vesicles increased with parasite maturation, reaching approximately 60% at the schizont stage, whereas CD81-positive vesicles showed comparatively little variation across the developmental stages.

Tetraspanin-positive populations were also detected in uRBC-derived sEV preparations (Fig. 2C). The proportions of CD9-, CD63- and CD81-positive vesicles were generally lower than those observed in iRBC-derived preparations, indicating differences in tetraspanin profiles between infected and uninfected erythrocyte-derived sEV populations.

Together, these findings indicate that *P. falciparum* infection is associated with a higher proportion of membrane-labelled particles and changes in the relative representation of tetraspanin-positive sEV populations throughout parasite development.

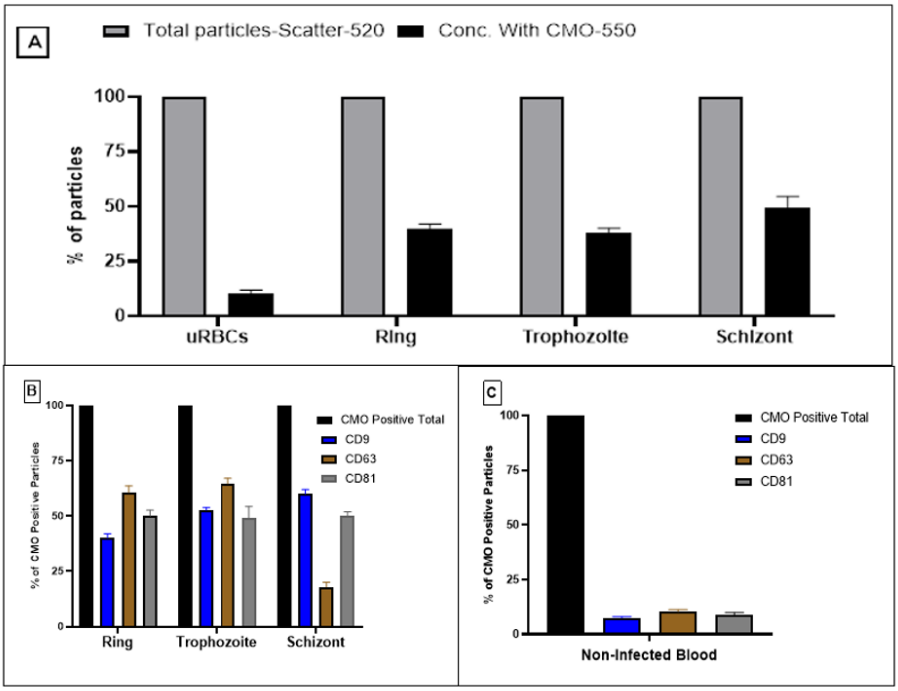

Figure 2. Fluorescence nanoparticle tracking analysis of membrane-bound and tetraspanin-positive small extracellular vesicle populations derived from *Plasmodium falciparum*-infected erythrocytes. (A) Percentage of CellMask Orange (CMO)-positive particles detected by fluorescence nanoparticle tracking analysis (fNTA) in small extracellular vesicle (sEV) preparations derived from uninfected red blood cells (uRBCs) and *P. falciparum*-infected red blood cells (iRBCs) at the ring, trophozoite and schizont stages. CMO-positive particles were quantified in fluorescence mode and expressed as a percentage of the total particle concentration measured in scatter mode (520 nm) for each preparation. **(B)** CD9-, CD63- and CD81-positive sEV populations in ring-, trophozoite- and schizont-stage iRBC preparations, expressed as a percentage of the corresponding total CMO-positive particle population. **(C)** CD9-, CD63- and CD81-positive sEV populations in uRBC-derived preparations, expressed as a percentage of the total CMO-positive particle population. Data are presented as mean ± SD from three independent biological replicates (n = 3).

Parasite-derived proteins are detected in sEVs from infected erythrocytes

Western blotting was performed to characterise the protein cargo of sEVs derived from uninfected red blood cells (uRBCs) and *P. falciparum*-infected red blood cells (iRBCs) at different developmental stages (Fig. 3). Flotillin-1, an EV-associated membrane protein commonly used as a positive marker for EVs, was detected in all sEV preparations, supporting the presence of extracellular vesicles in both uninfected and infected samples. In contrast, GM130, a Golgi-associated protein used as a negative marker to assess contamination with intracellular cellular components, was not detected in the sEV preparations.

The parasite-derived proteins *Plasmodium* aldolase and histidine-rich protein 2 (HRP2) were detected in sEVs derived from infected erythrocytes (Fig. 3). *Plasmodium* aldolase showed an increase in band intensity with parasite maturation, with the strongest signal observed in schizont-derived sEVs. In contrast, HRP2 was detected in sEVs from all infected stages, with the strongest signal observed in ring-derived sEVs. Neither parasite-derived protein was detected in uRBC-derived sEVs.

Together with the increased total protein concentration observed in schizont-derived sEVs (Fig. 1E), these findings suggest that sEVs released from infected erythrocytes are associated with parasite-derived proteins. The distinct stage-dependent patterns observed for aldolase and HRP2 further suggest that the parasite-derived protein composition of sEVs varies during parasite development.

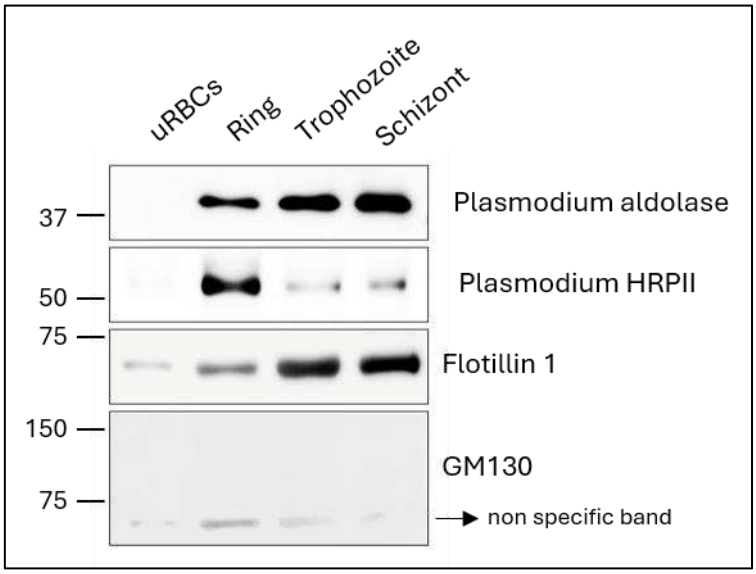

Figure 3. Detection of parasite-derived proteins in small extracellular vesicles by western-blotting. Western blot analysis of proteins associated with small extracellular vesicles (sEVs) isolated from uninfected red blood cells (uRBCs) and *Plasmodium falciparum*-infected red blood cells (iRBCs) at the ring, trophozoite and schizont stages. Membranes were probed for *Plasmodium* aldolase and histidine-rich protein 2 (HRP2) as parasite-derived proteins, flotillin-1 as an EV-associated marker, and GM130, a Golgi-associated protein, as a negative marker for cellular contamination. Representative blots from three independent biological replicates (n = 3). All uncropped original blots are provided as supplement.

RNA abundance and parasite-specific rRNAs in sEVs

Total and small RNA were detected in sEV preparations derived from uninfected and P. falciparum-infected erythrocytes (Fig. 4A–B). RNA concentrations varied across parasite developmental stages, with the highest levels observed in schizont-derived sEVs.

Proteinase K + RNase A treatment reduced both total and small RNA concentrations compared with untreated samples, indicating removal of externally exposed RNA, while a proportion of RNA remained detectable following treatment.

To determine whether the RNA protected within sEVs included parasite-derived RNA, P. falciparum-specific 28S and 18S rRNAs were analysed by RT-qPCR using RNA extracted from Proteinase K + RNase A-treated sEV samples (Fig. 4C–D). The relative abundance of both 28S and 18S rRNAs varied significantly across parasite developmental stages, with the highest levels observed in schizont-derived sEVs. These findings demonstrate pronounced enrichment of parasite-specific rRNAs in schizont-derived sEVs and support the presence of parasite-derived RNA protected within the vesicles.

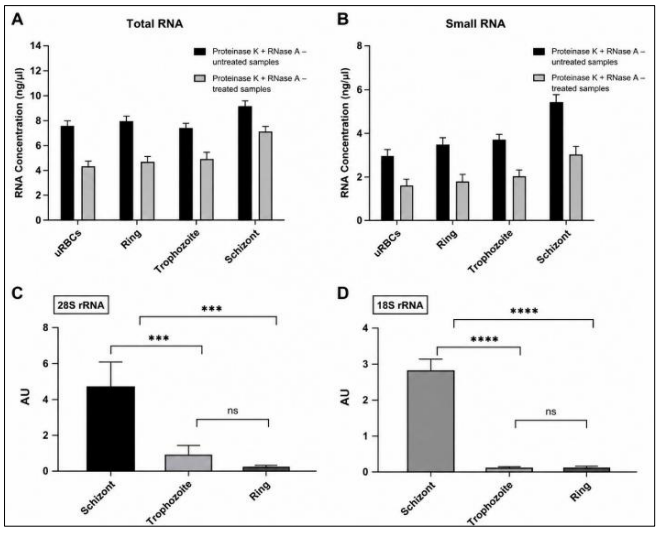

Figure 4. RNA abundance and *Plasmodium falciparum*-specific rRNAs in small extracellular vesicles derived from infected erythrocytes at distinct intraerythrocytic developmental stages. (A) Total RNA and (B) small RNA concentrations in sEVs derived from uninfected red blood cells (uRBCs) and ring-, trophozoite- and schizont-stage *P. falciparum*-infected red blood cells (iRBCs), analysed under untreated and Proteinase K + RNase A-treated conditions. (C) Relative abundance of *P. falciparum*-specific 28S rRNA and (D) 18S rRNA in Proteinase K + RNase A-treated sEV samples derived from ring-, trophozoite- and schizont-stage iRBCs, as determined by RT-qPCR. Relative abundance was calculated using the 2^−Ct method and scaled by factors of 10^8 for 28S rRNA and 10^{10} for 18S rRNA, with values expressed as arbitrary units (AU). Data are presented as mean ± SD from three independent biological replicates (n = 3). Statistical analysis was performed using ordinary one-way ANOVA followed by Tukey's multiple comparisons test. ****P < 0.0001; ***P < 0.001; ns, not significant.

Discussion

This study demonstrates that the abundance, membrane phenotype and molecular cargo of small extracellular vesicle (sEV)-enriched preparations derived from *Plasmodium falciparum*-infected erythrocytes vary across the intraerythrocytic developmental cycle. Importantly, these

changes extend beyond particle abundance to include differences in tetraspanin profiles and parasite-derived protein and RNA cargo. This is particularly relevant given the unusual biological characteristics of mature erythrocytes, which lack conventional secretory machinery. Previous studies have demonstrated that *P. falciparum*-infected erythrocytes release extracellular vesicles (EVs) containing host- and parasite-derived molecules that participate in parasite–parasite and parasite–host communication [14-20]. Our findings extend these observations by demonstrating stage-associated differences in particle abundance and molecular composition across defined developmental stages. The increased particle numbers, total protein concentration and relative abundance of parasite-specific 18S and 28S rRNAs observed at the schizont stage suggest that sEV-associated molecular signatures may provide information related to parasite development.

A notable finding was the increase in particle numbers in preparations derived from infected erythrocytes compared with uninfected controls, with the highest abundance observed at the schizont stage (Fig. 1A). Particle numbers also increased with increasing parasitaemia in schizont-stage cultures (Fig. 1B), indicating an association between parasite density and extracellular particle abundance. Previous studies have demonstrated that *P. falciparum*-infected erythrocytes release EVs involved in communication between parasites and interactions with host cells [14-18]. Mantel *et al.* demonstrated that infected erythrocyte-derived microvesicles participate in communication within the parasite population and with the host immune system [15], while Regev-Rudzki *et al.* reported the transfer of parasite-derived material between infected erythrocytes through exosome-like vesicles [16]. The present findings extend these observations by demonstrating that particle abundance differs across the ring, trophozoite and schizont stages and increases with parasite density.

The particularly high particle abundance at the schizont stage is biologically noteworthy. During schizogony, infected erythrocytes undergo extensive membrane remodelling as parasites complete replication and prepare for merozoite egress. These processes may contribute to changes in extracellular particle release. However, increased particle numbers should not be interpreted solely as evidence of actively regulated vesicle secretion, since membrane disruption or increased erythrocyte fragility during parasite maturation may also contribute to the detected particle population. Nevertheless, the association between parasite development, parasitaemia and changes in particle abundance indicates substantial alterations in extracellular particle populations during the intraerythrocytic cycle.

Physical characterisation supported the presence of an sEV-enriched population. Most detected particles were ≤200 nm (Fig. 1C), while transmission electron microscopy confirmed the presence of vesicular structures in both uninfected and infected erythrocyte-derived preparations (Fig. 1D). Total protein concentration was also higher in infected erythrocyte-derived preparations and reached its highest level at the schizont stage (Fig. 1E). Although increased protein concentration may reflect greater particle abundance, changes in protein cargo or the presence of co-isolated proteins, these findings are consistent with previous proteomic studies demonstrating that EVs released from *P. falciparum*-infected erythrocytes contain both host- and parasite-derived proteins [13,18,20]. Vimonpatranon *et al.* identified extensive host and parasite protein cargo in infected erythrocyte-derived EVs, including 128 *P. falciparum* proteins shared across the four EV groups examined [20]. These findings provide context for the increased protein content observed in our schizont-derived preparations.

Fluorescence nanoparticle tracking analysis (fNTA) provided further evidence of differences in membrane phenotype between infected and uninfected erythrocyte-derived preparations. CellMask Orange (CMO) labelling revealed that approximately 30–40% of particles in infected erythrocyte-derived preparations were CMO-positive, compared with approximately 10% in uninfected controls (Fig. 2A). Importantly, these percentages were calculated relative to the total particle concentration measured in scatter mode (520 nm) for each preparation. Therefore, they represent the proportion of membrane-labelled particles within each preparation rather than absolute vesicle abundance. The higher proportion of CMO-positive particles in infected preparations suggests that *P. falciparum* infection is associated with changes in the composition of the extracellular particle population, with a greater proportion of particles exhibiting detectable membrane labelling.

Further analysis revealed distinct stage-associated changes in tetraspanin-positive populations (Fig. 2B). CD63-positive vesicles accounted for approximately 65% of CMO-positive particles at the ring and trophozoite stages but decreased to approximately 18% at the schizont stage. In contrast, the proportion of CD9-positive vesicles increased during parasite maturation, reaching approximately 60% at the schizont stage, whereas CD81-positive populations showed comparatively little variation. Tetraspanin-positive vesicles were also detected in uninfected erythrocyte-derived preparations (Fig. 2C), demonstrating that these membrane-associated markers were not restricted to infected erythrocyte-derived vesicles. Together, these findings

559 suggest that *P. falciparum* infection and parasite development are associated with changes in
560 the relative representation of tetraspanin-positive vesicle populations.

561 The differences in CD9, CD63 and CD81 profiles may reflect parasite-associated changes in
562 erythrocyte membrane organisation or shifts in the composition of vesicle subpopulations
563 during parasite maturation. However, because mature erythrocytes lack the conventional
564 endosomal machinery present in nucleated cells, the detection of individual tetraspanins cannot
565 establish a classical exosomal biogenesis pathway. Furthermore, as tetraspanin-positive
566 populations were expressed relative to CMO-positive particles, the observed changes reflect
567 differences in their relative proportions rather than absolute numbers. These findings therefore
568 support the presence of phenotypic heterogeneity within the membrane-labelled sEV
569 population and suggest that parasite development influences the composition of these vesicles.

570 Protein analysis provided further evidence linking the sEV preparations to parasite infection.
571 *Plasmodium* aldolase and histidine-rich protein 2 (HRP2) were detected in infected
572 erythrocyte-derived sEV preparations but not in uninfected controls (Fig. 3). Notably, these
573 proteins displayed distinct stage-associated patterns. Aldolase showed its strongest western
574 blot signal in schizont-derived preparations, whereas HRP2 was detected across all infected
575 stages, with the strongest signal observed at the ring stage. These observations suggest that the
576 association of individual parasite proteins with sEV preparations varies during the
577 intraerythrocytic developmental cycle.

578 The detection of parasite-derived proteins is consistent with previous proteomic studies of EVs
579 released from *P. falciparum*-infected erythrocytes [20]. Vimonpatranon *et al.* identified
580 numerous parasite proteins in EVs derived from early- and late-stage infected erythrocytes,
581 including proteins associated with parasite invasion [20]. However, their developmental stages
582 were grouped into broader early- and late-stage populations rather than analysing ring,
583 trophozoite and schizont stages separately. The present study therefore extends these
584 observations by examining defined developmental stages and identifying distinct patterns for
585 individual parasite proteins.

586 The differing patterns of aldolase and HRP2 are particularly noteworthy. Previous studies have
587 demonstrated that PfHRP2 content increases during the erythrocytic cycle, with substantial
588 release occurring around schizont rupture [24]. In contrast, the strongest HRP2 signal in the
589 present sEV preparations was observed at the ring stage, while aldolase was most prominent at

the schizont stage. Thus, the stage-associated pattern of sEV-associated HRP2 did not appear to parallel either aldolase or overall particle abundance. This may indicate differences in the association of individual parasite proteins with extracellular vesicle populations during parasite development. However, as western blotting was qualitative, these findings should be interpreted cautiously. Quantitative densitometric analysis, with appropriate normalisation to an EV-associated marker such as flotillin-1, would help determine whether changes in parasite protein signals reflect differences in cargo abundance or variation in the vesicle population.

HRP2 is of particular interest because circulating PfHRP2 has been investigated as an indicator of total parasite biomass. Mature trophozoites and schizonts sequester within the microvasculature and are therefore poorly represented by peripheral parasitaemia [25]. Dondorp *et al.* demonstrated that PfHRP2-derived estimates of total parasite biomass were associated with disease severity [25]. Whether sEV-associated HRP2 provides additional information beyond soluble HRP2 remains unknown. Nevertheless, EVs may offer a complementary biomarker source because they can carry multiple molecular components, including proteins and nucleic acids, while their lipid bilayer may protect enclosed cargo from extracellular degradation [8-12]. The simultaneous detection of parasite-derived proteins and parasite-specific rRNAs in the present study supports further investigation of sEV-associated molecular signatures, although their diagnostic and prognostic value requires validation in clinical samples.

RNA analysis provided additional evidence of parasite-associated molecular cargo within the sEV preparations (Fig. 4). Total and small RNA concentrations were highest in schizont-derived preparations (Fig. 4A–B). Proteinase K and RNase A treatment reduced RNA concentrations, although a proportion remained detectable. This finding is consistent with the presence of RNA protected within vesicles or otherwise resistant to enzymatic degradation under the conditions used. Previous studies have also demonstrated that EVs released from *P. falciparum*-infected erythrocytes contain parasite-derived RNA [19].

Importantly, parasite-specific 18S and 28S rRNAs showed their highest relative abundance in schizont-derived preparations (Fig. 4C–D). As mature erythrocytes are enucleated and lack ribosomes, detection of *P. falciparum*-specific rRNAs provides a molecular link between the RNA detected in these preparations and parasite infection. Previous studies have identified parasite-derived RNA within EVs [19], while more recent small-RNA sequencing has demonstrated that environmental conditions can influence EV abundance and RNA cargo [26].

Our findings extend these observations by demonstrating developmental-stage-associated differences in two defined parasite-specific rRNAs.

The higher relative abundance of 18S and 28S rRNAs in schizont-derived preparations may have potential biomarker significance. Mature trophozoites and schizonts sequester within the microvasculature and are consequently underrepresented in peripheral blood. Extracellular molecular signatures associated with these developmental stages could potentially provide information about parasite populations that are not readily detected through conventional peripheral parasitaemia measurements. This concept is consistent with the rationale underlying the use of circulating PfHRP2 as an estimate of total parasite biomass [25]. However, the present study does not establish whether sEV-associated parasite rRNAs reflect total parasite biomass, sequestered parasite populations or differences in RNA content per vesicle. Further studies involving particle-normalised RNA measurements and clinical samples are required to address these questions.

This potential application may be particularly relevant to cerebral malaria, where sequestration of mature *P. falciparum*-infected erythrocytes within the cerebral microvasculature contributes to disease pathogenesis [4-7]. Recent clinical evidence also supports the broader potential of circulating EV cargo as a source of disease-associated molecular information. Kioko *et al.* demonstrated that plasma EV mRNA from children with cerebral malaria contained signatures associated with brain-derived and vascular cell populations and varied with disease trajectory and severity [27]. Although their study primarily examined host-derived transcripts rather than parasite-specific rRNAs, it supports further investigation of circulating EV cargo as a potential source of non-invasive biomarkers in cerebral malaria.

Together, the protein and RNA findings indicate that sEV-enriched preparations contain multiple parasite-associated molecular signatures. Combining parasite-derived proteins with parasite-specific nucleic acids may therefore provide a broader approach to biomarker development than relying on individual soluble parasite markers. However, the diagnostic significance of these molecules cannot be established from *in vitro* experiments alone, and their specificity, stability and clinical relevance require further investigation.

A strength of this study was the use of synchronised erythrocyte-only cultures representing defined ring, trophozoite and schizont stages. This minimised contributions from leukocytes and other nucleated host cells, allowing more confident attribution of parasite-specific

molecules to infected erythrocyte-derived preparations. The use of complementary techniques, including NTA, fNTA, TEM, protein quantification, western blotting and RNA analysis, also enabled characterisation of the preparations at morphological, membrane and molecular levels.

Several limitations should be acknowledged. This was an *in vitro* study using the K1 strain of *P. falciparum*, and the findings may not fully reflect the complex EV environment during natural infection. Although the isolation procedure enriched for small vesicles, complete separation from non-vesicular particles and soluble macromolecules cannot be assumed. Similarly, CMO labelling identifies membrane-labelled particles but does not independently establish vesicle purity or biogenesis. The analysis of tetraspanin-positive populations was based on their relative proportions within the CMO-positive population and therefore does not establish differences in their absolute abundance. Molecular analysis was restricted to selected parasite proteins and rRNAs rather than comprehensive proteomic or transcriptomic profiling. Furthermore, western blot analysis was qualitative, and RNA abundance was not normalised to particle number. Finally, the biological activity of the isolated sEVs was not investigated.

Future studies should validate these findings in clinical samples and determine whether sEV abundance and parasite-specific cargo correlate with parasitaemia, total parasite biomass, disease severity and treatment response. Quantitative analysis of parasite proteins, particle-normalised RNA measurements and comprehensive molecular profiling could identify additional stage-associated cargo. Functional studies could also establish whether sEVs released at different parasite stages exert distinct effects on endothelial or immune cells. Such investigations may be particularly relevant to cerebral malaria, where interactions between infected erythrocytes, vascular endothelium and inflammatory pathways contribute to microvascular pathology [4-7,27].

Conclusions:

In conclusion, the abundance, membrane phenotype and molecular composition of sEV-enriched preparations varied across the *P. falciparum* intraerythrocytic developmental cycle and with increasing parasitaemia. Schizont-derived preparations exhibited the highest particle numbers and total protein concentration, together with the highest relative abundance of parasite-specific 18S and 28S rRNAs. Fluorescence NTA revealed a higher proportion of CMO-positive particles in infected preparations and distinct stage-associated changes in CD9-

and CD63-positive populations. Parasite-derived proteins also displayed different patterns, with aldolase most prominent at the schizont stage and HRP2 at the ring stage. Together, these findings highlight the potential of sEV-associated molecular signatures as indicators of parasite infection and developmental stage. Further clinical validation is required to establish whether these signatures can contribute to monitoring parasite biomass, developmental stage and potentially sequestered parasite populations in *P. falciparum* malaria.

Declarations

Ethics approval and consent to participate

The study has been approved by the institutional ethics committee of the University of Salford (application ID: 8497; date of approval: 21/10/2022).

Consent for publication

All authors agree with this version of the manuscript and agree for submission towards publication.

Availability of data and materials

All source for the materials is mentioned within the manuscript and/or provided in the supplement.

Competing interests

The authors declare no competing interests.

Funding

The study is funded by the University of Salford Technicians Fund (project codes: ELGS-29 and SEGY-0020).

Authors' contributions

MA did all the experimental work and data analysis and wrote the first draft of the manuscript. BS provided expert support for western blots. TA provided expert support for EV

characterisation and gene expression studies. NN and AM had conceived the project and supervised the overall progress along resource management. All authors have contributed to the draft of the manuscript.

Acknowledgements

The authors gratefully acknowledge the University of Salford Technician Committee for providing partial funding for this project. We also thank Alex Couchman for technical support and the University of Salford sEV team, particularly Dr. Sowmya Chinta and Dr. Joseph Morgan, for their valuable technical assistance and support throughout the study.

References

1. World Health Organization. *World Malaria Report 2024*. Geneva: World Health Organization; 2024.

2. Gebreweld A, Erkihun Y, Feleke DG, Hailu G, Fiseha T. Thrombocytopenia as a diagnostic marker for malaria in patients with acute febrile illness. *J Trop Med.* 2021;2021:5585272.

3. Tangpukdee N, Duangdee C, Wilairatana P, Krudsood S. Malaria diagnosis: a brief review. *Korean J Parasitol.* 2009;47(2):93–102.

4. Miller LH, Baruch DI, Marsh K, Doumbo OK. The pathogenic basis of malaria. *Nature.* 2002;415(6872):673–679.

5. Storm J, Craig AG. Pathogenesis of cerebral malaria—inflammation and cytoadherence. *Front Cell Infect Microbiol.* 2014;4:100.

6. Smith JD, Rowe JA, Higgins MK, Lavstsen T. Malaria's deadly grip: cytoadhesion of *Plasmodium falciparum*-infected erythrocytes. *Cell Microbiol.* 2013;15(12):1976–1983.

7. Turner L, Lavstsen T, Berger SS, Wang CW, Petersen JEV, Avril M, et al. Severe malaria is associated with parasite binding to endothelial protein C receptor. *Nature.* 2013;498(7455):502–505.

8. Raposo G, Stoorvogel W. Extracellular vesicles: exosomes, microvesicles, and friends. *J Cell Biol.* 2013;200(4):373–383.

9. Théry C, Witwer KW, Aikawa E, Alcaraz MJ, Anderson JD, Andriantsitohaina R, et al. Minimal information for studies of extracellular vesicles 2018 (MISEV2018): a position

statement of the International Society for Extracellular Vesicles and update of the MISEV2014 guidelines. *J Extracell Vesicles.* 2018;7(1):1535750.

10. Yáñez-Mó M, Siljander PR, Andreu Z, Zavec AB, Borràs FE, Buzas EI, et al. Biological properties of extracellular vesicles and their physiological functions. *J Extracell Vesicles.* 2015;4:27066.

11. Kalluri R, LeBleu VS. The biology, function, and biomedical applications of exosomes. *Science.* 2020;367(6478):eaau6977.

12. Jung AL, Møller Jørgensen M, Bæk R, Artho M, Griss K, Han M, et al. Surface proteome of plasma extracellular vesicles as mechanistic and clinical biomarkers for malaria. *Infection.* 2023;51(5):1491–1501.

13. Dey S, Mohapatra S, Khokhar M, Hassan S, Pandey RK. Extracellular vesicles in malaria: shedding light on pathogenic depths. *ACS Infect Dis.* 2024;10(3):827–844.

14. Mantel PY, Marti M. The role of extracellular vesicles in *Plasmodium* and other protozoan parasites. *Cell Microbiol.* 2014;16(3):344–354.

15. Mantel PY, Hoang AN, Goldowitz I, Potashnikova D, Hamza B, Vorobjev I, et al. Malaria-infected erythrocyte-derived microvesicles mediate cellular communication within the parasite population and with the host immune system. *Cell Host Microbe.* 2013;13(5):521–534.

16. Regev-Rudzki N, Wilson DW, Carvalho TG, Sisquella X, Coleman BM, Rug M, et al. Cell-cell communication between malaria-infected red blood cells via exosome-like vesicles. *Cell.* 2013;153(5):1120–1133.

17. Sisquella X, Ofir-Birin Y, Pimentel MA, Cheng L, Abou Karam P, Sampaio NG, et al. Malaria parasite DNA-harbouring vesicles activate cytosolic immune sensors. *Nat Commun.* 2017;8(1):1985.

18. Sampaio NG, Cheng L, Eriksson EM. The role of extracellular vesicles in malaria biology and pathogenesis. *Malar J.* 2017;16(1):245.

19. Babatunde KA, Mbagwu S, Hernández-Castañeda MA, Adapa SR, Walch M, Filgueira L, et al. Malaria infected red blood cells release small regulatory RNAs through extracellular vesicles. *Sci Rep.* 2018;8(1):884.

20. Vimonpatranon S, Roytrakul S, Phaonakrop N, Lekmanee K, Atipimonpat A, Srimark N, et al. Extracellular vesicles derived from early and late stage *Plasmodium falciparum*-infected red blood cells contain invasion-associated proteins. *J Clin Med.* 2022;11(14):4250.

21. Aparici-Herraiz I, Gualdrón-López M, Castro-Cavadía CJ, Carmona-Fonseca J, Yasnot MF, Fernandez-Becerra C, et al. Antigen discovery in circulating extracellular vesicles from *Plasmodium vivax* patients. *Front Cell Infect Microbiol.* 2022;11:811390.

22. Baum J, Papenfuss AT, Mair GR, Janse CJ, Vlachou D, Waters AP, et al. Molecular genetics and comparative genomics reveal RNAi is not functional in malaria parasites. *Nucleic Acids Res.* 2009;37(11):3788–3798.

23. Grinev A, Fokina N, Bogomolov D, Berechikidze I, Lazareva Y. Prediction of gene expression regulation by human microRNAs in *Plasmodium falciparum*. *Genes Environ.* 2021;43(1):22.

24. Desakorn V, Dondorp AM, Silamut K, Pongtavornpinyo W, Sahassananda D, Chotivanich K, et al. Stage-dependent production and release of histidine-rich protein 2 by *Plasmodium falciparum*. *Trans R Soc Trop Med Hyg.* 2005;99(7):517–524. doi:10.1016/j.trstmh.2004.11.014.

25. Dondorp AM, Desakorn V, Pongtavornpinyo W, Sahassananda D, Silamut K, Chotivanich K, et al. Estimation of the total parasite biomass in acute falciparum malaria from plasma PfHRP2. *PLoS Med.* 2005;2(8):e204. doi:10.1371/journal.pmed.0020204.

26. Vetter L, Bajalan A, Ahamed MT, Scasso C, Shafeeq S, Andersson B, et al. Starvation induces changes in abundance and small RNA cargo of extracellular vesicles released from *Plasmodium falciparum*-infected red blood cells. *Sci Rep.* 2023;13:18423.

27. Kioko M, Mwangi S, Pance A, Ochola-Oyier LI, Kariuki S, Newton C, et al. The mRNA content of plasma extracellular vesicles provides a window into molecular processes in the brain during cerebral malaria. *Sci Adv.* 2024;10(33):eadl2256. doi:10.1126/sciadv.adl2256.

Supplementary Files

This is a list of supplementary files associated with this preprint. Click to download.

- AbubaketetalSupplementaryfigure.pdf